

CrossMark
click for updatesCite this: *Med. Chem. Commun.*, 2014, 5, 1634

Mechanism of forming trimer, self-assembling nano-particle and inhibiting tumor growth of small molecule CIPPCT†

Fengxiang Du,^a Xiaoyi Zhang,^a Shan Li,^a Yaonan Wang,^a Meiqing Zheng,^a Yuji Wang,^a Shurui Zhao,^a Jianhui Wu,^a Lin Gui,^a Ming Zhao^{*ab} and Shiqi Peng^{*a}

The mechanisms of small molecules forming nanospecies and the effect of the nanospecies of small molecules on their pharmacological actions remain to be elucidated. As one of our efforts here, a uPA inhibitor, (5a*S*,12*S*,14a*S*)-5,14-dioxo-12-(2-tryptophanylthreo-nylbenzylester-*N*-yl-ethyl-1-yl)-1,2,3,5,5a,6,11,12,14,14a-decahydro-5*H*,14*H*-pyrrolo[1,2:4,5]-pyrazino[1,2:1,6]pyrido[3,4-*b*]indole (CIPPCT) was presented. Energy-minimization, FT-MS and 2-D ROESY spectra defined CIPPCT taking III-like conformation, and the intermolecular association drove CIPPCT to form a finger ring-like trimer. Images from transmission electron, scanning electron and atomic force microscopies consistently visualized that in aqueous solution at pH 6.7 and 10⁻¹⁰ M concentration, CIPPCT generally assembled nanoparticles of 9–67 nm in diameter. Mesoscale simulation demonstrated that a nanoparticle 9.4 nm in diameter contained 350 trimers. *In vivo* CIPPCT dose-dependently inhibited tumor growth in S180 mice. An ELISA assay confirmed that CIPPCT concentration-dependently downregulated serum uPA. The nanoparticles of CIPPCT are capable of occurring in mouse plasma and adhering on HeLa cells, and nanosized CIPPCT directly correlates the downregulation of uPA with inhibition of tumor growth.

Received 4th April 2014
Accepted 20th June 2014

DOI: 10.1039/c4md00158c

www.rsc.org/medchemcomm

Introduction

Biological nanosystems have been perspective viewed.^{1–3} To prepare the nanospecies and characterize the properties of the nanomaterials, various technologies have been developed^{4–11} that effectively promote the development of nanomedicine.^{12–15} Regarding nanomedicine, the progress of the nanotechnology in the past decades mainly occurred in the preparation of drug delivery systems, such as liposomes.^{16,17} Recently, the self-assembly of single small molecules at the nanoscale,^{18,19} and the effect of the self-assembly of some small molecules on their biological properties has attracted intense interest.^{20,21} Based on these advances, some bioactive small molecules capable of self-assembly have been used in the functionalization of metal surfaces,²² in the crafting of functional biological materials,²³ and in the increase of anti-osteoporosis activity.²⁴ The physical and chemical mechanisms of small molecules forming nano-species, as well as the effect of the nanospecies of small molecules on their pharmacological actions, remain to be elucidated.

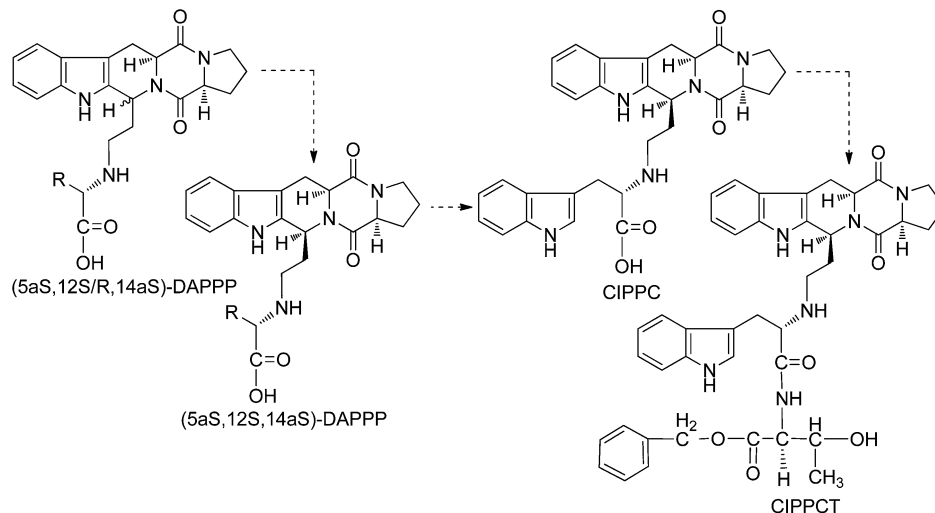
In various physiological processes related to tissue remodeling, the plasminogen activator (PA) system is of importance. The PA system consists of PAI-1/PAI-2 (the inhibitors of PA), a urokinase-type plasminogen activator (uPA), the receptor of uPA (uPAR) and the plasminogen (the substrate of uPAR).²⁵ Regarding physiology, PAI-1 is a primary inhibitor of plasminogen activation in hemostasis and is one of the main regulators of the fibrinolytic system.²⁶ Abnormal expression of the PAI-1 gene induces different diseases, including fibrosis, obesity, cancer and vascular disease.^{27,28} Moreover, regarding carcinogenesis, upregulation of the PAI-1 gene results in the inhibition of tumor progression and correlates with a less aggressive phenotype of some cancers, presumably due to the inhibition of the uPA activity.^{27,29,30} The elevated level of PAI-1 in several primary malignant tumors, such as breast, gastric and ovarian cancers, as well as adenocarcinomas of lung, is considered as their marker.^{27,28,31} On the other hand, a high level of PAI-2 in a tumour is associated with improved prognoses. In the presence of PAI-1, PAI-2 inhibits uPA, whereas in the presence of vitronectin, PAI-2 inhibits adherent cells. In inhibiting uPA, the elevated level of PAI-2 in a tumour microenvironment outcompetes PAI-1.³²

Depending on the interactions of uPA with endogenous PAI-1, it exerts dual effects on tumor progression. In murine models, a stable overexpression of uPA promotes the growth of colon tumors that naturally express high PAI-1, but inhibits the growth of renal tumors that naturally express low PAI-1.³³ In a

^aCollege of Pharmaceutical Sciences, Capital Medical University, Beijing 100069, P.R. China. E-mail: sqpeng@bjmu.edu.cn; mingzhao@bjmu.edu.cn; Fax: +86-10-8391-1528; +86-10-8280-2482; Tel: +86-10-8391-1528; +86-10-8280-2482

^bDepartment of Biomedical Science and Environmental Biology, Kaohsiung Medical University, Kaohsiung, Taiwan

† Electronic supplementary information (ESI) available: NMR spectra of CIPPCT were included. See DOI: 10.1039/c4md00158c



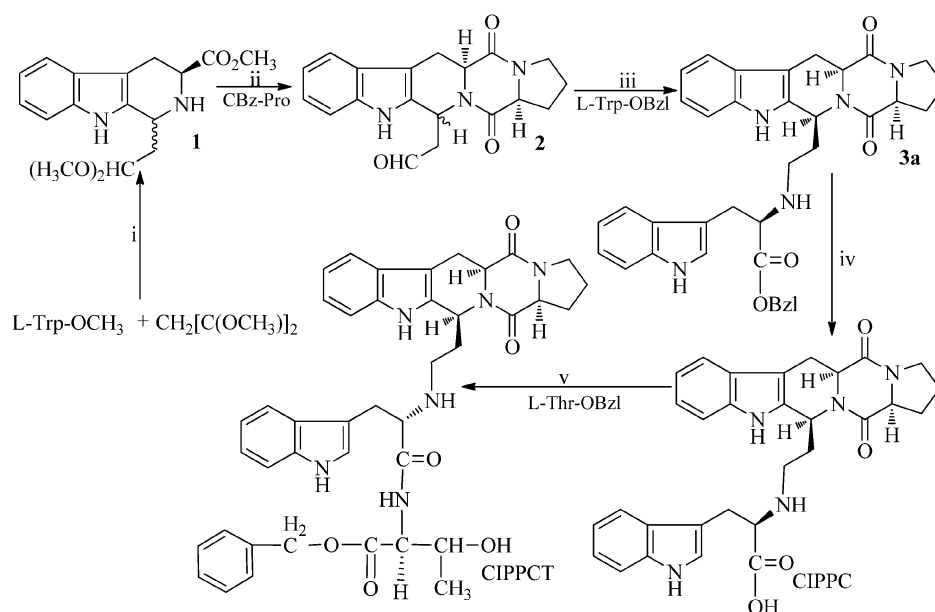
Scheme 1 Discovery course of CIPPCT.

variety of malignant tumours, the overexpression of uPA and/or uPAR has been strongly correlated with poor prognosis. Impairing the function of uPA and/or uPAR, or inhibiting the expression of uPA and/or uPAR, limits the metastatic potential of many tumours.³⁴ Clinical and experimental evidence proves the significance of uPA and/or uPAR for a number of solid cancers, and the downregulation of uPA and/or uPAR is considered a potential strategy in cancer therapy.^{35,36}

Perturbing the interaction between uPA and uPAR has attracted some interest, and a few novel compounds have been provided for inhibiting uPA. In a preliminary structure-activity exploration, amiloride analogs that inhibited uPA were synthesized.³⁷ The *N*-nicotinonitrile derivatives that allegedly perturb the interaction between uPA and uPAR failed to affect

the expression of uPA.³⁸ Wider investigations are needed to successfully discover relevant lead compounds.

The course of discovering CIPPCT is depicted in Scheme 1. The (5a*S*,12*S*,14a*S*)-isomers of (5a*S*,12*S*/*R*,14a*S*)-5,14-dioxo-12-(2-aminoacid-*N*-ylethyl-1-yl)-1,2,3,5,5a,6,11,12,14,14a-decahydro-5*H*,14*H*-pyrolo[1,2:4,5]pyrazino[1,2:1,6]pyrido[3,4-*b*]indoles (DAPPP) were previously explored as inhibitors of urokinase.³⁹ Of (5a*S*,12*S*,14a*S*)-DAPPP analogs, the 2-trptophan-*N*-ylethyl-1-yl derivative (CIPPC) more effectively antagonized the thrombolytic activity of urokinase, which provided a lead to a uPA inhibitor.⁴⁰ Of Trp-Trp-AA-OBzl, Trp-Trp-Thr-OBzl possessed the highest anti-tumor activity, which provided a possible modification of CIPPC with Trp-Thr-OBzl.⁴¹ In the formation of nanoparticles WY3-56, a PAD4 inhibitor, the intermolecular



Scheme 2 Synthetic route of CIPPCT.

π - π interactions were found to be essential that provided an effective approach in designing nanoscale self-assembly.^{42,43} Based on this information, a uPA inhibitor (5aS,12S,14aS)-5,14-dioxo-12-(2-tryptophanylthreo-nylbenzylester-*N*-ylethyl-1-yl)-1,2,3,5,5a,6,11,12,14,14a-decahydro-5*H*,14*H*-pyrolo[1,2:4,5]pyrazino[1,2:1,6]pyrido[3,4-*b*]indole (CIPPCT) was designed to investigate the mechanisms of nanoparticle formation with FT-MS and 2-D ROESY spectra, to visualize the feature of the nanoparticles with transmission electron, scanning electron and atomic force microscopies, and to correlate the bioactivity with the nanoparticles with the *in vitro* and the *in vivo* assays.

Experimental

Synthesis

To conveniently obtain CIPPCT, a 5-step reaction sequence of Scheme 2 was used, which can be divided into steps 1–3 for preparing **3a**, and steps 4 and 5 for preparing CIPPCT.

(i) CH₃OH, hydrochloric acid, 45 °C; (ii) SOCl₂, CH₂Cl₂, diisopropylamine; (iii) DMF, Et₃N, anhydrous Na₂SO₄, KBH₄, CH₃OH and (iv) DMF, DCC, anhydrous Na₂SO₄, *N*-methylmorpholine.

The preparation of the compounds are described in following section; NMR spectra are available in the ESI.†

Preparing 1-(2,2-dimethoxyethyl)-1,2,3,4-tetrahydrocarboline-3-carboxylic acid methyl ester (1). A suspension of 5.0 g *L*-tryptophan methyl ester (24.5 mmol) and 6.0 mL 1,1,3,3-tetramethoxypropane (23.6 mmol) in 50 mL CH₃OH was adjusted to pH 2 with hydrochloric acid (5 M) and stirred at 45 °C for 48 h. The reaction mixture was evaporated *in vacuo* to remove the solvent, the residue was diluted with 50 mL water, and the formed solution was extracted 3 times with 30 mL ethyl acetate. Further, the extracts were combined and successively washed with 10% aqueous Na₂CO₃ (3 × 30 mL) and saturated aqueous NaCl (2 × 30 mL), then dried over anhydrous Na₂SO₄, filtered and concentrated *in vacuo* to provide **1**. ESI-MS (*m/z*): 319 [M + H]⁺.

Preparing (5aS,12S/R,14aS)-5,14-dioxo-12-cabonylmethyl-1,2,3,5,5a,6,11,12,14,14a-decahydro-5*H*,14*H*-pyrolo[1,2:4,5]pyrazino[1,2:1,6]pyrido[3,4-*b*]indole (2). To 5.0 g CBz-*L*-Pro (14.8 mmol), 50 mL SOCl₂ was added dropwise, and the reaction mixture was heated for 5 h reflux. The mixture was concentrated *in vacuo* to remove excess SOCl₂, and the residue was treated with 30 mL ether to provide CBz-protected prolinyl chloride as colorless powder, to which a solution of 3.2 g 1-(2,2-dimethoxyethyl)-1,2,3,4-tetrahydrocarboline-3-carboxylic acid methyl ester (**1**, 10 mmol) in 50 mL CH₂Cl₂ was added at 0 °C and stirred for 0.5 h. The reaction mixture was adjusted to pH 9 with diisopropylamine and stirred at room temperature for 24 h. The reaction mixture was concentrated *in vacuo*, the residue was dissolved in 150 mL acetone, and the solution was treated with 200 mg *p*-TsOH. After stirring at 45 °C for 1 h, the reaction mixture was treated with 5 mL Et₃N and concentrated *in vacuo*; the residue was purified by column chromatography (CHCl₃/CH₃OH, 40 : 1). The fraction of interest was evaporated *in vacuo*, and the residue was recrystallized from acetone to provide 1.5 g (29%) of the title compound. ESI-MS (*m/z*): 338 [M + H]⁺.

Preparing (5aS,12S,14aS)- and (5aS,12R,14aS)-5,14-dioxo-12-(2-tryptophan-benzylester-*N*-ylethyl-1-yl)-1,2,3,5,5a,6,11,12,14,14a-decahydro-5*H*,14*H*-pyrolo[1,2:4,5]pyrazino[1,2:1,6]pyrido[3,4-*b*]indoles (3a** and **3b**).** To a solution of 2.3 g (5aS,12S/R,14aS)-5,14-dioxo-12-cabonylmethyl-1,2,3,5,5a,6,11, 12, 14,14a-decahydro-5*H*,14*H*-pyrolo[1,2:4,5]pyrazino[1,2:1,6]pyrido[3,4-*b*]indole (**2**, 6.8 mmol) in 10 mL DMF was added 2.4 g HCl·Trp-OBzl (6.8 mmol), 1.5 mL Et₃N and 6 g anhydrous Na₂SO₄. The reaction mixture was stirred at room temperature for 3 h, added to a solution of 1 g KBH₄ (18.4 mmol) in 10 mL CH₃OH, and stirred for another 1 h. The reaction mixture was evaporated *in vacuo*, and the residue was dissolved with 40 mL ethyl acetate and 20 mL deionized water. The two-phase solution was treated with 2 mL hydrochloric acid (5 M) to decompose the excess KBH₄, and adjusted to pH 9 with aqua ammonia NH₃ (5 M). The ethyl acetate phase was separated, and the aqueous phase was extracted with ethyl acetate (3 × 40 mL). The combined ethyl acetate phases were washed with 40 mL saturated aqueous NaCl, dried with anhydrous Na₂SO₄, filtered and concentrated *in vacuo*. The residue was then purified and separated on column chromatography (CHCl₃/CH₃OH, 30 : 1) to give 1.3 g (61%) **3a** and 1.5 g (71%) **3b**.

3a. FT-MS (*m/z*): 615.2830 [M]⁺; mp:175–176 °C; ¹HNMR (300 MHz, CDCl₃): δ = 8.223 (s, 1H), 7.756–7.584 (dd, *J* = 7.5 Hz, *J* = 7.5 Hz, 2H), 7.494–7.411 (m, 3H), 7.411(m, 3H), 7.386–7.317 (m, 5H), 7.155–7.149 (m, 3H), 7.05 (m, 1H), 6.084–6.057 (d, *J* = 8, 1 Hz, 1H), 5.538–5.488 (q, *J* = 4.8 Hz, 5.1 Hz, 1H), 5.216 (s, 2H), 4.174 (m, 1H), 4.106 (m, 1H), 4.004–3.988(d, *J* = 4.8 Hz, 1H), 3.559–3.542 (m, 1H), 3.434–3.288(td, *J* = 5.1 Hz, *J* = 3.0 Hz, *J* = 3.0 Hz, 2H), 2.959–2.910 (m, 2H), 2.886–2.757 (m, 2H), 2.743–2.655 (m, 1H), 2.466–2.376 (m, 1H), 2.318–2.198 (m, 2H), 2.098–1.913 (m, 2H); ¹³C NMR (75 MHz, CDCl₃): δ = 173.86, 169.48, 165.90, 165.83, 156.14, 136.34, 135.96, 135.71, 135.38, 133.96, 133.53, 129.60, 128.61, 128.34, 128.21, 126.99, 126.10, 125.66, 123.71, 122.59, 122.13, 121.39, 120.30, 120.12, 120.01, 119.41, 118.88, 118.17, 117.66, 115.44, 112.07, 111.83, 111.43, 111.23, 106.39, 105.70, 66.68, 62.21, 59.34, 59.19, 58.89, 57.40, 56.95, 50.28, 49.14, 46.24, 45.37, 44.46, 40.43, 35.44, 29.51, 28.64, 28.54, 23.24, 23.12, 21.41, 21.23, 10.00; IR (KBr): 3308, 2978, 2954, 2880, 1659, 1454, 1398, 1335, 1236, 1096, 745 cm⁻¹. In the ROESY 2D NMR spectrum, a positive NOE signal between 5aS-H and 12-H was observed.

3b. FT-MS (*m/z*): 615.2845 [M]⁺; mp:105–106 °C; ¹HNMR (300 MHz, CDCl₃): δ = 11.087 (s, 1H), 10.677 (s, 1H), 7.458–7.404 (dd, *J* = 4.8 Hz, *J* = 5.2 Hz, 2H), 7.295–7.250 (m, 7H), 7.075–6.935 (m, 4H), 6.068–6.040 (dd, *J* = 1.8 Hz, *J* = 1.8 Hz, 1H), 5.216–5.134(dt, *J* = 7.8 Hz, *J* = 7.8 Hz, 2H), 4.765–4.734 (dd, *J* = 2.7 Hz, *J* = 2.4 Hz, 1H), 4.258–4.235 (d, *J* = 6.9 Hz, 1H), 4.193–4.138(m, 2H), 3.806–3.790 (m, 1H), 3.428–3.388(dd, *J* = 2.7 Hz, *J* = 2.7 Hz, 2H), 3.333 (m, 4H) 3.012–2.982 (m, 2H), 2.875–2.727 (m, 1H), 2.407–2.361(t, *J* = 6.9 Hz, *J* = 6.9 Hz, 1H), 2.226–2.209 (t, *J* = 2.4 Hz, 2.7 Hz, 1H), 2.176–2.124 (m, 1H), 1.934–1.918 (m, 1H), 1.855–1.788 (m, 2H); ¹³C NMR (75 MHz, CDCl₃): δ = 174.03, 165.51, 164.42, 136.66, 136.55, 136.29, 135.99, 133.66, 128.81, 128.29, 127.82, 127.13, 126.58, 121.68, 121.14, 119.23, 118.82, 118.26, 118.02, 111.61, 111.25, 106.00, 105.56, 66.04, 58.77, 53.54, 52.90, 46.90,

46.40, 45.06, 29.93, 28.63, 25.22, 21.46; IR (KBr): 3251, 3233, 2957, 2930, 2857, 1659, 1454, 1398, 1150, 748 cm^{-1} . In the ROESY 2D NMR spectrum, no NOE signal between 5aS-H and 12-H was observed.

Preparing (5aS,12S,14aS)-5,14-dioxo-12-(2-tryptophan-*N*-ylethyl-1-yl)-1,2,3,5,5a,6,11,12,14,14a-decahydro-5H,14H-pyrolo-[1,2:4,5]pyrazino[1,2:1,6]pyrido[3,4-*b*]-indoles (CIPPC). To a solution of 1.3 g (5aS,12S,14aS)-5,14-dioxo-12-(2-tryptophan-benzylester-*N*-ylethyl-1-yl)-1,2,3,5,5a,6,11,12,14,14a-decahydro-5H,14H-pyrolo-[1,2:4,5]pyrazino[1,2:1,6]-pyrido[3,4-*b*]indoles (**3a**, 2.1 mmol) in 5 mL methanol aqueous, NaOH (4 M) was added dropwise to adjust the pH to 12, and the reaction mixture was stirred at room temperature for 2 h. The reaction mixture was adjusted to pH 5 with hydrochloric acid (2 M), evaporated under vacuum, and the residue was purified on silica gel column to provide 863 mg (90%) of CIPPC. ESI-MS (m/z): 526 $[\text{M} + \text{H}]^+$; ^1H NMR (400 MHz, DMSO), $\delta(\text{ppm}) = 11.27$ (s, 1H), 10.86 (s, 1H), 7.54 (dd, $J = 7.6$, $J = 7.6$ Hz, 2H), 7.33 (m, 2H), 7.13 (s, 1H), 7.06 (s, 2H), 6.92 (t, $J = 7.2$ Hz, 1H), 5.38 (s, 1H), 4.50 (s, 1H), 4.29 (m, 2H), 3.45–3.34 (m, 4H), 3.24 (s, 1H), 3.15 (m, 2H), 2.83 (m, 1H), 2.51 (s, 1H), 2.22 (s, 1H), 1.98–1.79 (m, 5H). ^{13}C NMR (100 MHz, DMSO), $\delta(\text{ppm}) = 171.11$, 170.44, 165.55, 136.34, 136.00, 133.98, 125.95, 124.11, 121.65, 118.64, 118.47, 118.19, 111, 71, 111.47, 109.49, 105.53, 101.53, 63.10, 62.17, 58.69, 56.32, 52.87, 49.42, 45.03, 43.18, 40.37, 40.16, 39.95, 36.27, 34.60, 28.21, 26.75, 22.93, 21.33. IR (KBr): 3390.86, 3269.34, 3113, 3057, 3014, 2954, 2933, 2877, 1640, 1465, 1303, 1130, 1103, 1008, 762, 702 cm^{-1} .

Preparing (5aS,12S,14aS)-5,14-dioxo-12-(2-tryptophanyl-threoninebenzylester-*N*-ylethyl-1-yl)-1,2,3,5,5a,6,11,12,14,14a-decahydro-5H,14H-pyrolo[1,2:4,5]pyrazino[1,2:1,6]pyrido-[3,4-*b*]-indoles (CIPPCT). To a solution of 120 mg (0.23 mmol) CIPPC and 77 mg (0.23 mmol) Thr-OBzl in 15 mL anhydrous DMF 100 mg (0.46 mmol), DCC and 30 mg anhydrous Na_2SO_4 were added. The reaction mixture was adjusted to pH 9 with *N*-methylmorpholine, and stirred at room temperature for 1 h. The reaction mixture was evaporated under vacuum, the residue was dissolved in 20 mL ethyl acetate, the solution was washed with 10% aqueous Na_2CO_3 (15 mL \times 3) and dried with anhydrous Na_2SO_4 . After filtration the filtrate was evaporated under vacuum, and the residue was purified on a silica gel column to provide 129 mg (78%) CIPPCT as yellow powder. Mp 127–128 $^\circ\text{C}$. $[\alpha]_D^{20} = -191$ ($c = 0.6$, CH_2Cl_2). FT-MS(m/z): 717.33161 $[\text{M} + \text{H}]^+$. ^1H NMR (300 MHz, CDCl_3): $\delta(\text{ppm}) = 8.27$ (s, 1H), 8.02 (t, $J = 5.4$ Hz, 1H), 7.974 (d, $J = 7.8$ Hz, 1H), 7.464 (m, 2H), 7.364 (m, 5H), 7.319 (d, $J = 2.1$ Hz, 1H), 7.173 (m, 2H), 7.120 (m, 1H), 6.128 (s, 1H), 5.186 (s, 2H), 4.264 (d, $J = 6.6$ Hz, 1H), 4.240 (m, 1H), 4.203 (d, $J = 6.6$ Hz, 1H), 4.040 (d, $J = 4.8$ Hz, 1H), 3.964 (m, 1H), 3.879 (dd, $J = 5.1$ Hz, $J = 7.2$ Hz, 1H), 3.768 (m, 1H), 3.630 (m, 2H), 3.490 (m, 1H), 3.350 (m, $J = 5.1$ Hz, 1H), 2.900 (m, 2H), 2.511 (m, 2H), 2.467 (m, 2H), 2.241 (m, 1H), 2.005 (m, 3H), 1.241 (dd, $J = 4.2$ Hz, $J = 7.2$ Hz, 3H). ^{13}C NMR (75 MHz, CDCl_3): $\delta(\text{ppm}) = 171.1$, 170.7, 165.8, 162.6, 136.5, 135.6, 135.2, 133.8, 128.6, 128.5, 128.4, 127.6, 127.0, 125.8, 124.9, 122.5, 121.8, 119.9, 119.8, 119.4, 117.9, 112.0, 111.4, 105.7, 68.2, 67.3, 65.3, 60.7, 60.4, 59.3, 57.4, 48.0, 46.1, 45.2, 42.8, 36.5, 35.1, 31.4, 29.7, 29.6, 28.6, 23.3, 21.0, 20.8, 20.0, 14.2, 8.6. IR (KBr): 3387, 3325,

2974, 2928, 2884, 1742, 1649, 1520, 1454, 1402, 1339, 1196, 1111, 745, 845 cm^{-1} .

Generation of energy-minimized conformation

CIPPCT was sketched in ChemDraw 10.0, converted to 3D conformation in Chem3D 10.0 and then energy-minimized in Discovery Studio 3.5 with an MMFF force field. The energy-minimized conformation was utilized as the starting conformation for conformation generation. The energy-minimized conformations of CIPPCT were sampled in the whole conformational space *via* systematic search and BEST methods in Discovery Studio 3.5. Both the systematic search and BEST methods were practiced with SMART minimizer using a CHARMM force field. In addition, the energy threshold was set to 20 kcal mol^{-1} at 300 K. The maximum number of minimization steps was set to 200 and the minimization RMS gradient was set to 0.1 Å. The maximum generated conformations were set to 255 with a RMSD cutoff 0.2 Å.

Measuring two-dimensional ROESY spectra

The one-dimensional ^1H NMR spectrum of 10 mg CIPPCT in 0.5 mL deuterated dimethyl sulfoxide (DMSO- d_6) was measured on a Bruker 800 MHz spectrometer. The probe temperature was regulated to 298 K. Using a simple pulse-acquire sequence zg30, the spectra were recorded. To ensure full relaxation of the ^1H resonances, typical acquisition parameters consisted of 64 K points covering a sweep width of 16447 Hz, a pulse width (pw90) of 8.63 μs and a total repetition time of 24 s were used. Before Fourier transformation, the digital zero filling to 64 K and a 0.3 Hz exponential function were applied to FID. The resonance at 2.5 ppm indicated an impurity ($\text{CD}_2\text{HSOCD}_2\text{H}$) in the residual solvents, and tetramethylsilane (TMS) was used as internal reference. Standard absorptive two-dimensional ^1H - ^1H chemical shift correlation spectra (COSY) were tested with the same spectrometer. Each spectrum consisted of a matrix of 2 K (F2) by 0.5 K (F1) covering a sweep width of 9615.4 Hz. Before Fourier transformation, the matrix was zero filled to 1 K by 1 K, and the standard sinebell apodization functions were applied in both dimensions. Two-dimensional ROESY experiments were carried out in the phase-sensitive mode using the same spectrometer. Each spectrum consisted of a matrix of 2 K (F2) by 1 K (F1) and covered a sweep width of 9615.4 Hz. Spectra were obtained using spin-lock mixing periods of 200 ms. Before Fourier transformation, the matrix was zero filled to 1 K by 1 K, and q sine apodization functions were applied in both dimensions.

Measuring FT-MS spectra

ESI mass spectra of CIPPCT were measured on a solarix FT-ICR mass spectrometer (Bruker Daltonics, Billerica, MA, USA) consisting of an ESI/MALDI dual ion source and a 9.4 T superconductive magnet. The measurements were performed with the positive MALDI ion mode. The ion source was a Smart-beam-II laser (wavelength, 355 nm; focus setting, 'medium'; repetition rate, 1000 Hz). The QCID mass was set to 2150.98172 m/z , and the isolation window was 5 m/z . Data were collected using

solariXcontrol software. Spectral data were processed with Data Analysis software (Bruker Daltonics).

Measuring TEM images

Shape and size measurements of CIPPCT nanospecies were performed using transmission electron microscopy (TEM; JSM-6360 LV, JEOL, Tokyo, Japan). An aqueous solution of CIPPCT (pH 6.7, 10^{-10} M) was dripped onto a formvar-coated copper grid, to which a drop of anhydrous ethanol was added to promote the removal of water. The grid was allowed to dry thoroughly in air and then was heated at 35 °C for 24 h. The copper grids were viewed under TEM. The shape and size distributions of the nanospecies were determined by counting >100 species in randomly selected regions on the copper grid. All determinations were carried out on triplicate grids and at 80 kV (the electron beam accelerating voltage). Images were recorded on an imaging plate (Gatan Bioscan Camera Model 1792, Pleasanton, CA, USA) with 20 eV energy windows at 6000–400 000 \times and were digitally enlarged.

Measuring SEM images

The shape and size of lyophilized powders of CIPPCT (from a solution of CIPPCT in ultrapure water) were measured by scanning electron microscopy (SEM, JEM-1230, JEOL, Tokyo, Japan) at 50 kV. The lyophilized powders were attached to a copper plate with double-sided tape (Euromedex, Strasbourg, France). The specimens were coated with 20 nm gold-palladium using a Joel JFC-1600 Auto Fine Coater. The coater was operated at 15 kV, 30 mA, and 200 mTorr (argon) for 60 s. The shape and size distributions of the lyophilized powders of CIPPCT were measured by examining >100 particles in randomly selected regions on the SEM alloy. All measurements were performed on triplicate copper plates. Images were recorded on an imaging plate (Gatan Bioscan Camera Model 1792) with 20 eV energy windows at 100–10 000 \times and were digitally enlarged.

Measuring AFM images

Atomic force microscopy (AFM) images of contact mode were recorded on a Nanoscope 3D AFM (Veeco Metrology, Santa Barbara, CA, USA) under ambient conditions. Samples of CIPPCT in water (pH 6.7, 10^{-10} M) were used for recording the images.

Theoretically predicting nanoparticle size

The mesoscale simulation software was used to perform the calculation and to predict how many trimers of CIPPCT can construct the smallest nanoparticle revealed by TEM. Discover module of the Materials Studio software was used for the simulation. CIPPCT molecule was built and optimized simply in the Visualizer window. “Beads” were constructed from atomistic simulations and placed at the center-of-mass of groups of atoms corresponding to particular parts of the CIPPCT molecule.

In vitro anti-proliferation assay

In vitro cell viability assays were carried out using 96-well microtiter culture plates and MTT [3-(4,5-dimethylthiazol-2-yl)-

2,5-diphenyltetrazolium bromide] staining according to standard procedures. HL-60, HT-29, HeLa, SW480 and HepG2 cells (5×10^3 cells per well) were grown in RPMI-1640 or DMEM medium [containing 10% (v/v) fetal calf serum, $60 \mu\text{g mL}^{-1}$ penicillin, and $100 \mu\text{g mL}^{-1}$ streptomycin]. Stock solutions of CIPPCT were prepared in DMSO and diluted with culture medium to the desired concentration. Cultures were propagated at 37 °C in a humidified atmosphere (with 5% CO₂) for 24 h, and then CIPPCT was added (final concentrations were 0, 1, 5, 10, 25, 50 and 100 μM). After 48 h of treatment, MTT solution was added ($5 \mu\text{g mL}^{-1}$; 25 μL per well), and cells were incubated for an additional 4 h. After adding 100 μL of DMSO to dissolve the MTT-formazan product, the optical density was measured at 570 nm by a microplate reader ($n = 6$).

In vivo anti-tumor assay

Following the protocol review and approval by the ethics committee of Capital Medical University, the investigations were performed. The committee assures that the welfare of mice was maintained in accordance with the requirements of the animal welfare act. Male ICR mice (22 ± 2 g, purchased from Capital Medical University) were maintained at 21 °C with a natural day/night cycle in a conventional animal colony. Mice were 10 weeks old at the beginning of the experiment. S180 ascites tumor cells were subcutaneously injected to form solid tumors. To initiate subcutaneous tumors, cells obtained in ascitic form from tumor-bearing mice were serially transplanted once per week. Subcutaneous tumors were implanted under the skin at the right armpit by injecting 0.2 mL of NS (normal saline) containing 1×10^7 viable tumor cells. Twenty-four hours after implantation, mice were randomly divided into treatment, positive control and vehicle control groups (7 per group). For treatment groups CIPPCT in 0.2 mL of 0.3% carmellose sodium (CMC-Na) was orally administered at 4.0, 0.8 and 0.16 $\mu\text{mol kg}^{-1}$ per dose. For the positive control group, doxorubicin in NS was intraperitoneally injected at 2 $\mu\text{mol kg}^{-1}$ per dose. For vehicle control, 0.2 mL of CMC-Na (0.3%, negative control) was orally administered. Oral administrations for treated groups or for vehicle control or intraperitoneal injections for positive control were administered every day for 7 days, and mice were weighed daily. Twenty-four hours after the last administration, the mice were weighed and blood sampled from eyes; they were then sacrificed by ether anesthesia and dissected to immediately obtain and weigh the tumor and organ samples.

uPA ELISA assay

uPA level in the serum of S180 mice treated with CIPPCT at 4, 0.8 and 0.15 $\mu\text{mol kg}^{-1}$ per dose was measured by enzyme immunoassay according to the manufacturer's instructions (mouse uPA ELISA kit, Usen Life Science Inc., Wuhan). In brief, 24 h after the last administration, mouse blood was collected in 3.8% aqueous solution of sodium citrate from the eyes, kept at room temperature for 30 min, centrifuged at 3000 rpm for 20 min; the separated serum was kept at -20 °C before use. In the ELISA assay, murine monoclonal antibody specific for uPA was coated on the 96-well microplate. Each standard and serum sample was

added to the plate and incubated. After washing away unbound proteins, enzyme-linked antibody specific for uPA was added to the wells. Absorbency was measured at 492 nm, and the detection limit was 100 pg mL⁻¹. All samples were run in duplicate. The variations of intra- and inter-assays were less than 10%.

Results and discussion

Energy-minimization and III-like conformation

A III-like conformation of CIPPCT was generated in computer-assisted molecular modeling. The systematic search method produced 30 conformations, and the BEST method produced 203 conformations. The 233 generated conformations were visually examined, and the conformation having the lowest free energy was selected. This conformation has a -35.06 kcal mol⁻¹ relative energy to the starting conformation. Regarding the steric relationship between pyrolo[1,2:4,5]pyrazino[1,2:1,6]pyrido[3,4-*b*]indole, tryptophan and benzyl moieties, CIPPCT had a III-like conformation, in which the distance from pyrrole-H of pyrolo[1,2:4,5]pyrazino[1,2:1,6]pyrido[3,4-*b*]indole moiety to the α -H of tryptophan moiety was 2.298 Å, which was reflected by cross-peak a in the ROESY 2D NMR spectrum (see Fig. 2b).

FT-MS spectroscopy and trimer

The intermolecular association of CIPPCT was explored with FT-MS spectrum (Fig. 2a). This spectrum showed three interesting

ions. The ion 717.33161 (bearing one positive charge) represents the mass of a CIPPCT monomer (theoretical value: 716.3322) plus H. The ion 1433.66550 (bearing one positive charge) represents the mass of a CIPPCT dimer (theoretical value: 1432.6644) plus H. The ion 2149.96613 (bearing one positive charge) represents the mass of a CIPPCT trimer (theoretical value: 2148.9966) plus H. Furthermore, the monomer ion was characterized by the highest peak among the 3 ions. To clarify the correlation of the monomer, the dimer and the trimer, a qCID spectrum was measured and inserted into Fig. 2a. The qCID spectrum demonstrated that the dimer and the monomer were derived from the fragmentation of the trimer under FT-MS conditions. Therefore, the spectra support the interpretation that the intermolecular association leads to trimerization and in aqueous CIPPCT exists as the trimer.

ROESY 2D NMR spectrum and trimerization manner

The pattern of the intermolecular association was identified with the ROESY 2D NMR spectrum. In Fig. 2b, the ROESY-related three cross-peaks are labeled with blue circles. Of the three cross-peaks, the cross-peak a was assigned for the interaction of the pyrrole-H in pyrolo[1,2:4,5]pyrazino[1,2:1,6]pyrido[3,4-*b*]indole moiety with the α -H of tryptophan moiety and reflected the steric relationship of two intramolecular H, according to the low energy conformation of Fig. 1. The cross-peak b was assigned for the interaction of the H of CH₂ in benzyl moiety with the 13-H in pyrolo[1,2:4,5]pyrazino[1,2:1,6]pyrido[3,4-*b*]indole moiety; according to the low energy conformation of Fig. 1, this interaction can only result from two intermolecular H. The cross-peak c was assigned for the interaction of the 19-H in pyrolo[1,2:4,5]pyrazino[1,2:1,6]pyrido[3,4-*b*]indole moiety with the α -H of threonine moiety; according to the low energy conformation defined in Fig. 1, this interaction can also only result from two intermolecular H. To fit the requirements of cross-peaks b and c, three CIPPCT molecules could associate in a manner shown in Fig. 2c and form a finger ring-like species. The data of NMR and MS together supported the interpretation that CIPPCT existed as finger ring-like trimer.

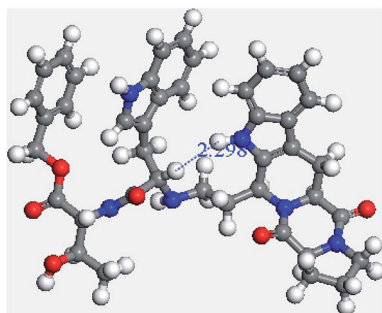


Fig. 1 A III-like conformation, the energy-minimized conformation.

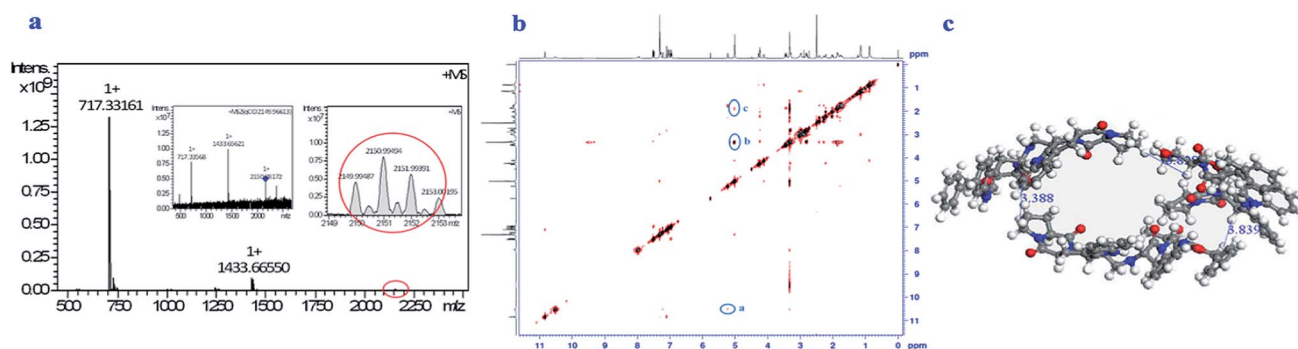


Fig. 2 (a) Ion peak in the FT-MS spectrum supporting trimerization of CIPPCT (bearing one positive charge, 2149.96613). The inset shows a qCID spectrum, indicating that monomers and dimers result from fragmentation of the trimer under FT-MS conditions. (b) ROESY 2D NMR spectrum: three cross-peaks indicating the intermolecular associations of CIPPCT (labeled with blue circles). (c) Finger ring-like trimer of CIPPCT, deduced from the ROESY 2D NMR and FT-MS spectra, in which the distance of the hydrogens in the cross-peaks b and c are indicated.

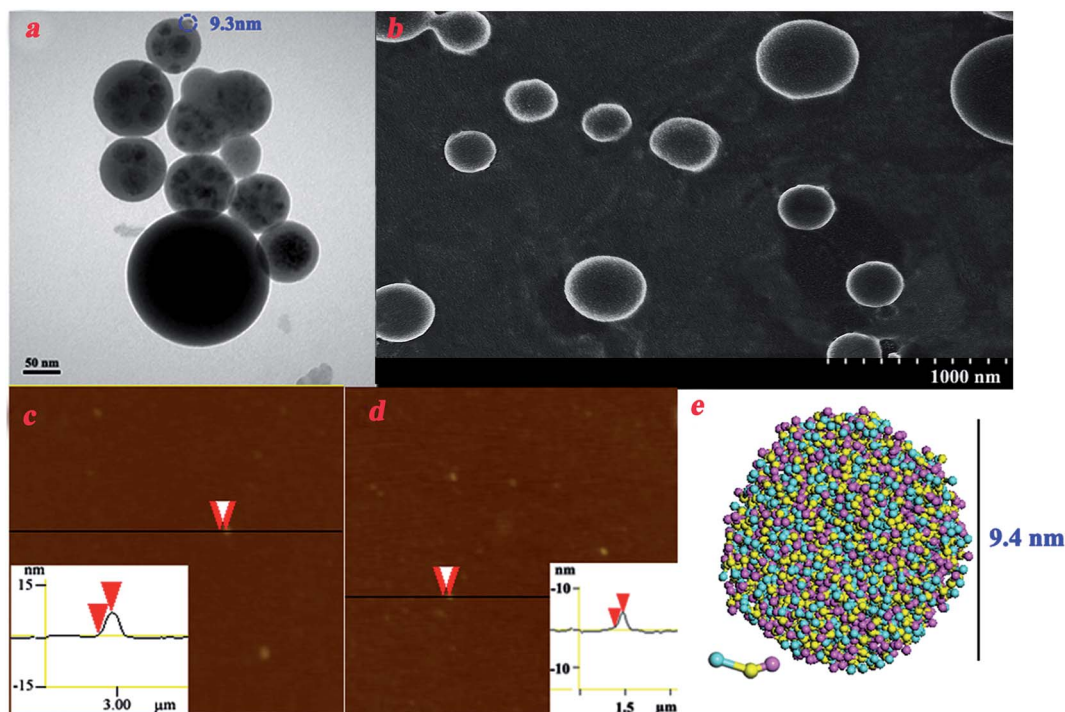


Fig. 3 TEM, SEM and AFM images, as well as mesoscale simulation software, assisted calculation of the nanoparticles of CIPPCT. (a) TEM images of CIPPCT in pH 6.7 and 10^{-10} M aqueous solution. (b) SEM images of powders of CIPPCT precipitated from pH 6.7 and 10^{-10} M aqueous solution. (c and d) AFM images of CIPPCT precipitated from pH 6.7 and 10^{-10} M aqueous solution. (e) Mesoscale simulation software-assisted calculation of the structure of CIPPCT nanoparticles. CIPPCTs were divided into three beads. The green, yellow and pink beads represented pyrrolo[1,2:4,5]-pyrazino[1,2:1,6]pyrido[3,4-*b*]indole, tryptophan and threonine moieties, respectively.

TEM, SEM, AFM and nano-particles

The nano-structure was shown using TEM, SEM and AFM images. The TEM image of Fig. 3a revealed that in an aqueous solution of pH 6.7, and 10^{-10} M concentration CIPPCT formed nanoparticles of 9–194 nm in diameter, and the diameter of most particles was less than 125 nm. SEM images of Fig. 3b revealed that the precipitates from the aqueous solution of pH 6.7 and 10^{-10} M concentration were the nanoparticles of 27–67 nm in diameter, and the diameter of most particles was less than 47 nm. AFM images of Fig. 3c and d revealed that the precipitates from an aqueous solution of pH 6.7 and 10^{-10} M concentration were nanoparticles of 74–79 nm in diameter. Therefore all images of TEM, SEM and AFM consistently visualized that in 10^{-10} M aqueous solution CIPPCT existed as nano-particles, while the spectra of FT-MS and ROESY 2D NMR implied that the nano-particles were assembled by the trimers of CIPPCT.

Theoretical prediction and trimer number in nanoparticle

Mesoscale simulation predicted that the trimers of CIPPCT spontaneously formed nanoparticles and a nanoparticle of 9.4 nm in diameter contained 350 trimers (Fig. 3e). As seen in Fig. 3a, the smallest nanoparticle had a diameter of 9.3 nm. The consistency of the theoretically predicted nanoparticle with the experimentally tested nanoparticle emphasizes the utility of the theoretical prediction. In addition, this prediction provided an

approach to quantitatively estimate the number of the trimers for an optimal nanoparticle.

IC₅₀ for inhibiting cancer cell proliferation

The cytotoxicity of CIPPCT to HL60, HT29, HeLa, SW480 and HepG2 cells was examined using the MTT method, represented with IC₅₀ values, and is shown in Fig. 4a. In the MTT assays, the IC₅₀ values in inhibiting HeLa and SW480 cells were more than 100 μM, the IC₅₀ value in inhibiting HepG2 cells was more than 60 μM, the IC₅₀ value in inhibiting HT29 cells was more than 20 μM, and the IC₅₀ value in inhibiting HL60 cells was more than 10 μM. The relative higher IC₅₀ values suggest CIPPCT had low cytotoxicity and should not be a cytotoxic agent.

Dose-dependent inhibition for tumor growth

The *in vivo* anti-tumor activity of CIPPCT was assayed on an S180 mouse model, represented by tumor weight, and are shown in Fig. 4b. The assays led CIPPCT to exhibit an orally dose-dependent inhibition and to having a low effective dose at 0.16 μmol kg⁻¹. With respect to 4 μmol kg⁻¹ oral dose, CIPPCT had the same efficacy as the 2 μmol kg⁻¹ of intraperitoneally injected doxorubicin, suggesting that an oral administration of CIPPCT can offer desirable therapeutic effectiveness.

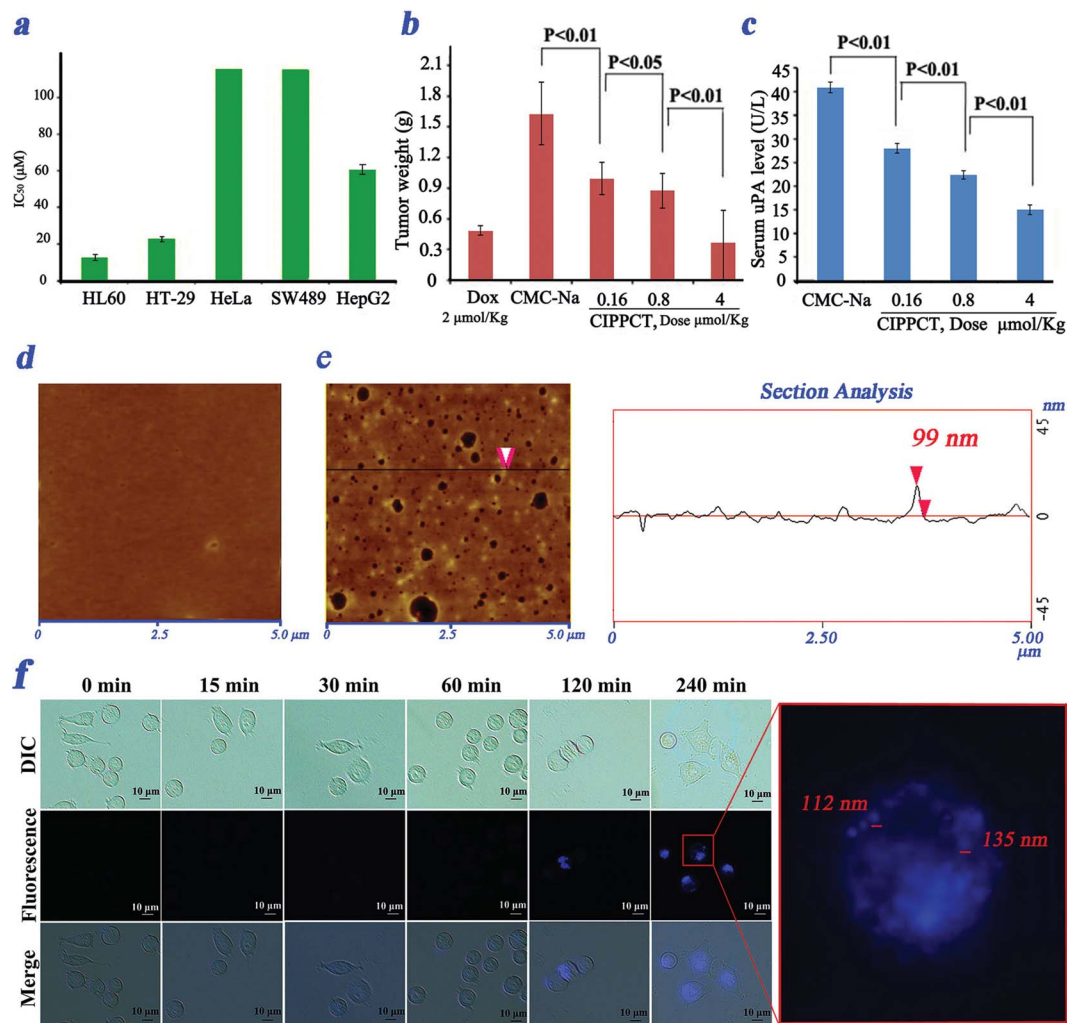


Fig. 4 CIPPCT possessed bioactivity on molecular, cell and animal models. (a) IC₅₀ of CIPPCT in inhibiting cancer cell proliferation, $n = 6$; (b) *In vivo* CIPPCT dose-dependently inhibiting tumor growth, $n = 10$; (c) *In vivo* CIPPCT dose-dependently decreasing serum uPA level, $n = 10$; (d) AFM image of mouse plasma alone; (e) AFM image of mouse plasma with CIPPCT; (f) fluorescence images demonstrating the time-dependent adherence of CIPPCT nanoparticles onto the surface of HeLa cells.

uPA levels in serum of mice treated with CIPPCT

The anti-tumor mechanism of CIPPCT was monitored with ELISA experiments; the uPA levels in the serum treated with 4.0, 0.8 and 0.16 $\mu\text{mol kg}^{-1}$ of oral CIPPCT are shown in Fig. 4c. In a variety of malignant tumours, the overexpression of uPA has been strongly correlated with poor prognosis. Experimental evidence proved that the downregulation of uPA could be considered a potential strategy in cancer therapy.^{11,12} CIPPCT dose-dependently decreased uPA levels in the serum of mice, reflecting CIPPCT dose-dependently downregulated uPA expression and suggested that by targeting uPA, CIPPCT inhibited tumor growth.

AFM of CIPPCT nanoparticles in mouse plasma

To visualize the morphological features of CIPPCT in the blood, an AFM test was performed on a Nanoscope 3D AFM (Veeco). Using the contact mode, the images of mouse plasma alone (negative control) and CIPPCT in mouse plasma (10^{-10} M, pH7.4)

were recorded. The images in Fig. 4e show that in mouse plasma, the nanoparticles of CIPPCT are 99 nm in diameter, whereas the mouse plasma gives no comparable nanoparticle (Fig. 4d).

Time-dependent adherence of CIPPCT nanoparticles onto the surface of HeLa cells

With a 282 nm excitation wave, CIPPCT can emit blue fluorescence at 418 nm, and this spectrum property was used to monitor the nanoparticles. In this case, CIPPCT nanoparticles on the cell surface were characterized by fluorescence images (Fig. 4f). When tumorigenic cells, HepG2, were treated with CIPPCT (10^{-10} M), the blue fluorescent nanoparticles of 100–135 nm in diameter steadily increased as the treatment time lengthened from 15 min to 240 min and especially as it went beyond 60 min.

Conclusion

In conclusion, with energy-minimization simulation, FT-MS spectra, ¹H NMR Noesy spectra, and images of TEM, SEM and

AFM, the chemical and physical mechanism of CIPPCT-forming nanoparticles could be clarified. ELISA, anti-proliferation and tumor growth assays provided evidence that downregulating uPA was the pharmacological mechanism by which CIPPCT inhibited tumor growth, benefited the increase of anti-tumor activity and decreased cytotoxicity.

Contribution of each author

The contribution of each author made to the manuscript mechanism of forming trimer, self-assembling nanoparticle and inhibiting tumor growth of small molecule CIPPCT is as follows: chemical synthesis, *in vivo* anti-tumor assay and uPA ELISA assay. Dr Fengxiang Du; mesoscale simulation and figures: Dr Xiaoyi Zhang; *in vitro* anti-proliferation assay: Dr Shan Li; MS, NMR and AFM data testing: Yaonan Wang, Meiqing Zheng and Shurui Zhao; MS/NMR data collection and interpretation: Dr Yuji Wang; literature search: Dr Jianhui Wu; TEM and SEM measuring: Dr Lin Gui; experimental design: Dr Ming Zhao; research guidance and paper writing: Dr Shiqi Peng.

Conflict of interest

The authors declare no competing financial interest.

Acknowledgements

This work was supported by the Beijing area major laboratory of peptide and small molecular drugs, the Project of Construction of Innovative Teams and Teacher Career Development for Universities and Colleges Under Beijing Municipality, the Natural Science Foundation (81373265 and 81270046), Beijing Natural Science Foundation (7112016 and 7132032) and Beijing Municipal Science & Technology Commission (Z141100002114049).

References

- W. Guannan and S. Xingguang, The synthesis and bio-applications of magnetic and fluorescent bifunctional composite nanoparticles, *Analyst*, 2011, **136**, 1783–1798.
- N. Kaji, Y. Okamoto, M. Tokeshi and Y. Baba, Nanopillar, nanoball, and nanofibers for highly efficient analysis of biomolecules, *Chem. Soc. Rev.*, 2010, **39**, 948–956.
- J. E. Gagner, S. Shrivastava, X. Qian, J. S. Dordick and R. W. Siegel, Amphiphile nanoarchitectonics: from basic physical chemistry to advanced applications, *Phys. Chem. Chem. Phys.*, 2013, **15**, 10580–10611.
- K. Taekyeong, J. Ki-Seok, H. Kwang, K. Hyung Min, P. Juhun, S. Yung Doug and H. Seunghun, Multilayered nano-prism vertex tips for tip-enhanced Raman spectroscopy and imaging, *Analyst*, 2013, **138**, 5588–5593.
- F. Meng and Z. Zhong, Polymersomes spanning from nano- to microscales: advanced vehicles for controlled drug delivery and robust vesicles for virus and cell mimicking, *J. Phys. Chem. Lett.*, 2011, **2**, 1533–1539.
- W. Chunyana and S. Valiyaveetil, Correlation of biocapping agents with cytotoxic effects of silver nanoparticles on human tumor cells, *RSC Adv.*, 2013, **3**, 14329–14338.
- B. Luan and R. Zhou, Nanopore-based sensors for detecting toxicity of a carbon nanotube to proteins, *J. Phys. Chem. Lett.*, 2012, **3**, 2337–2341.
- Y. Hongbin, F. Haiyu, W. Xiaohan and Y. Shuhong, Hierarchical assembly of micro-/nano-building blocks: bio-inspired rigid structural functional materials, *Chem. Soc. Rev.*, 2011, **40**, 3764–3785.
- S. P. Anthony and S. M. Draper, Nano/microstructure fabrication of functional organic material: Polymorphic structure and tunable luminescence, *J. Phys. Chem. C*, 2010, **114**, 11708–11716.
- R. Sood, C. Iojoiu, E. Espuche, F. Gouanveé, G. Gebel, H. Mendil-Jakani, S. Lyonnard and J. Jestin, Proton conducting ionic liquid doped nafion membranes: Nano-structuration, transport properties and water sorption, *J. Phys. Chem. C*, 2012, **116**, 24413–24423.
- R. H. Chou, S. C. Hsieh, Y. L. Yu, M. H. Huang, Y. C. Huang and Y. H. Hsieh, Fisetin inhibits migration and invasion of human cervical cancer cells by down-regulating urokinase plasminogen activator expression through suppressing the p38 MAPK-dependent NF- κ B signaling pathway, *PLoS One*, 2013, **8**, e71983.
- A. H. Mekki, D. L. Morris and M. H. Pourgholami, Urokinase plasminogen activator system as a potential target for cancer therapy, *Future Oncol.*, 2009, **5**, 1487–1499.
- B. Mishra, B. B. Patel and S. Tiwari, Colloidal nanocarriers: A review on formulation technology, types and applications toward targeted drug delivery, *Nanomedicine*, 2010, **6**, 9–24.
- D. B. Khadka and D. T. Haynie, Protein- and peptide-based electrospun nanofibers in medical biomaterials, *Nanomedicine*, 2012, **8**, 1242–1262.
- A. Rangnekar, A. M. Zhang, S. S. Li, K. M. Bompiani, M. N. Hansen, K. V. Gothelf, B. A. Sullenger and T. H. LaBean, Increased anticoagulant activity of thrombin-binding DNA aptamers by nanoscale organization on DNA nanostructures, *Nanomedicine*, 2012, **8**, 673–681.
- E. S. Kawasaki and T. A. Player, Nanotechnology, nanomedicine, and the development of new, effective therapies for cancer, *Nanomedicine*, 2005, **1**, 101–109.
- P. Sundaram, J. Wower and M. E. Byrne, A nanoscale drug delivery carrier using nucleic acid aptamers for extended release of therapeutic, *Nanomedicine*, 2012, **8**, 1143–1151.
- L. Li, G. Cui, M. Zhao, Y. Wang, H. Wang, W. Li and S. Peng, Assembly of β -cyclo-dextrin with 3S-tetrahydro- β -carboline-3-carboxylic acid and self-assembly of 6-(3S-carboline-3-carboxylaminoethylamino)-6-deoxy- β -cyclodextrin: Approaches to enhance antioxidation stability and anti-thrombotic potency, *J. Phys. Chem. B*, 2008, **112**, 12139–12147.
- X. Ren, G. Cui, M. Zhao, C. Wang and S. Peng, Coordination of thrombolytic Pro-Ala-Lys peptides with Cu (II): Leading to nano-scale self-assembly, increase of thrombolytic activity and additional vasodilation, *J. Phys. Chem. B*, 2008, **112**, 8174–8180.

- 20 A. Abelein, L. Lang, C. Lendel, A. Gräslund and J. Danielsson, Transient small molecule interactions kinetically modulate amyloid β peptide self-assembly, *FEBS Lett.*, 2012, **586**, 3991–3995.
- 21 A. Sood, M. Abid, S. Hailemichael, M. Foster, B. Török and M. Török, Effect of chirality of small molecule organofluorine inhibitors of amyloid self-assembly on inhibitor potency, *Bioorg. Med. Chem. Lett.*, 2009, **19**, 6931–6934.
- 22 A. Kühnle, Self-assembly of organic molecules at metal surfaces, *Curr. Opin. Colloid Interface Sci.*, 2009, **14**, 157–168.
- 23 J. B. Matson, R. H. Zha and S. I. Stupp, Peptide self-assembly for crafting functional biological materials, *Curr. Opin. Solid State Mater. Sci.*, 2011, **15**, 225–235.
- 24 Y. Wang, J. Wu, G. Kang, M. Zhao, L. Gui, N. Li, L. Peng, X. Zhang, L. Li and S. Peng, Novel nano-materials, RGD-tetrapeptide-modified 17 β -amino-11 α -hydroxyandrost-1,4-diene-3-one: Synthesis, self-assembly based nano-images and in vivo anti-osteoporosis evaluation, *J. Mater. Chem.*, 2012, **22**, 4652–4659.
- 25 M. Persson and A. Kjaer, Urokinase-type plasminogen activator receptor (uPAR) as a promising new imaging target: potential clinical applications, *Clin. Physiol. Funct. Imaging*, 2013, **33**, 329–337.
- 26 C. Dellas and D. J. Loskutoff, Historical analysis of PAI-1 from its discovery to its potential role in cell motility and disease, *Thromb. Haemostasis*, 2005, **93**, 631–640.
- 27 P. A. Andreasen, PAI-1-a potential therapeutic target in cancer, *Curr. Drug Targets*, 2007, **8**, 1030–1041.
- 28 M. W. Gramling and F. C. Church, Plasminogen activator inhibitor-1 is an aggregate response factor with pleiotropic effects on cell signaling in vascular disease and the tumor microenvironment, *Thromb. Res.*, 2010, **125**, 377–381.
- 29 K. Bajou, V. Masson, R. D. Gerard, P. M. Schmitt, V. Albert, M. Praus, L. R. Lund, T. L. Frandsen, N. Brunner, K. Dano, N. E. Fusenig, U. Weidle, G. Carmeliet, D. Loskutoff, D. Collen, P. Carmeliet, J. M. Foidart and A. Noël, The plasminogen activator inhibitor PAI-1 controls in vivo tumor vascularization by interaction with proteases, not vitronectin: implications for antiangiogenic strategies, *J. Cell Biol.*, 2001, **152**, 777–784.
- 30 G. A. McMahon, E. Petitclerc, S. Stefansson, E. Smith, M. K. Wong, R. J. Westrick, D. Ginsburg, P. C. Brooks and D. A. Lawrence, Plasminogen activator inhibitor-1 regulates tumor growth and angiogenesis, *J. Biol. Chem.*, 2001, **276**, 33964–33968.
- 31 M. K. Durand, J. S. Bødker, A. Christensen, D. M. Dupont, M. Hansen, J. K. Jensen, S. Kjølgaard, L. Mathiasen, K. E. Pedersen, S. Skeldal, T. Wind and P. A. Andreasen, Plasminogen activator inhibitor-I and tumour growth, invasion, and metastasis, *Thromb. Haemostasis*, 2004, **91**, 438–449.
- 32 S. Lobov and M. Ranson, Molecular competition between plasminogen activator inhibitors type-1 and -2 for urokinase: Implications for cellular proteolysis and adhesion in cancer, *Cancer Lett.*, 2011, **303**, 118–127.
- 33 Y. Jing, K. Kovacs, V. Kurisetty, Z. Jiang, N. Tsinoremas and J. R. Merchan, Role of plasminogen activator inhibitor-1 in urokinase's paradoxical in vivo tumor suppressing or promoting effects, *Mol. Cancer Res.*, 2012, **10**, 1271–1281.
- 34 V. Pillay, C. R. Dass and P. F. M. Choong, The urokinase plasminogen activator receptor as a gene therapy target for cancer, *Trends Biotechnol.*, 2006, **25**, 33–39.
- 35 C. E. de Bock and Y. Wang, Clinical significance of urokinase-type plasminogen activator receptor (uPAR) expression in cancer, *Med. Res. Rev.*, 2004, **24**, 13–39.
- 36 A. P. Mazar, The urokinase plasminogen activator receptor (uPAR) as a target for the diagnosis and therapy of cancer, *Anti-Cancer Drugs*, 2001, **12**, 387–400.
- 37 H. Matthews, M. Ranson, J. D. A. Tyndall and M. J. Kelso, Synthesis and preliminary evaluation of amiloride analogs as inhibitors of the urokinase-type plasminogen activator (uPA), *Bioorg. Med. Chem. Lett.*, 2011, **21**, 6760–6766.
- 38 A. H. Shamroukh, M. El-Shahat, J. Drabowicz, M. M. Ali, A. E. Rashad and H. S. Ali, Anticancer evaluation of some newly synthesized N-nicotinonitrile derivative, *Eur. J. Med. Chem.*, 2013, **69**, 521–526.
- 39 J. Liu, Y. Wang, Y. Yang, X. Jiang, M. Zhao, W. Wang, G. Wu, J. Wu, M. Zheng and S. Peng, Pyrolo[1,2:4,5]-1,4-dioxopyrazino[1,2:1,6]pyrido[3,4-b]indoles: A group of urokinase inhibitors, their synthesis and stereochemistry-dependent activity, *ChemMedChem*, 2011, **6**, 2312–2322.
- 40 S. Mei, J. Liu, M. Zhao, W. Wang, Y. Wang, G. Wu, M. Zheng and S. Peng, From Cerius² based stereoview to mouse and enzyme: The model systems for discovery of novel urokinase inhibitors, *Mol. Biosyst.*, 2011, **7**, 2664–2669.
- 41 X. Zhang, Y. Yang, M. Zhao, L. Liu, M. Zheng, Y. Wang, J. Wu and S. Peng, A class of Trp-Trp-AA-OBzl: Synthesis, *in vitro* anti-proliferation/*in vivo* anti-tumor evaluation, intercalation-mechanism investigation and 3D QSAR analysis, *Eur. J. Med. Chem.*, 2011, **46**, 3410–3419.
- 42 H. Zhu, Y. Wang, Y. Wang, S. i. Zhao, M. Zhao, L. Gui, W. Xu, X. Chen, Y. Wang and S. Peng, Folded conformation, cyclic pentamer, nano-structure and PAD4 binding mode of YW3-56, *J. Phys. Chem. C*, 2013, **117**, 10070–10078.
- 43 S. Jin, Y. Wang, H. Zhu, Y. Wang, S. Zhao, M. Zhao, J. Liu, J. Wu, W. Gao and S. Peng, Nano-Sized Aspirin-Arg-Gly-Asp-Val: Delivery of aspirin to thrombus by a target carrier Arg-Gly-Asp-Val tetrapeptide, *ACS Nano*, 2013, **7**, 7664–7673.